Human-robot collaborative object transfer using human motion prediction based on Dynamic Movement Primitives

Antonis Sidiropoulos[1,a], Yiannis Karayiannidis[2,b] and Zoe Doulgeri[1,c]

***Abstract*— This work focuses on the prediction of the human's motion in a collaborative human-robot object transfer with the aim of assisting the human and minimizing his/her effort. The desired pattern of motion is learned from a human demonstration and is encoded with a DMP (Dynamic Movement Primitive). During the object transfer to unknown targets, a model reference with a DMP-based control input and an EKF-based (Extended Kalman Filter) observer for predicting the target and temporal scaling is used. Global boundedness under the emergence of bounded forces with bounded energy is proved. The object dynamics are assumed known. The validation of the proposed approach is performed through experiments using a Kuka LWR4+ robot equipped with an ATI sensor at its end-effector.**

I. INTRODUCTION

The field of robotics has exhibited remarkable progress over the past years and the idea of having robots work collaborative with humans has gained a lot of ground. Tasks like lifting or carrying heavy objects occur quite frequently in everyday life and require combined effort and collaboration. Endowing human-like capabilities to robots that will allow them to manipulate objects in collaboration with humans in a shared environment is extremely beneficial both in industrial and household environments [1]. However, such an endeavor poses many challenges. Accurate synchronization between the robot and human partner and the negotiation of a common trajectory are indispensable for performing the task in a good synergy.

Specifically, in the case of collaborative object transfer, a physical coupling is established between the two partners through which interaction forces emerge. Disagreement between the partners' intention with respect to the target position of the object and the desired time duration will result in higher interaction forces [2]. A major issue in the field of human-robot interaction for assistance to manipulation is transparency. This basic feature qualifies the capacity of a robot to follow human movements without any human-perceptible resistive forces [3].

Human motion prediction has been proposed as a means to improve human robot collaboration. The use of the minimum jerk model for the human motion based on which the robot predicted the human motion was adopted in [4], [5], [6]. However, the minimum jerk model has been show to be unsuitable for manipulation tasks [2]. Another keenly advocated approach in the literature to tackle the pHRI problem is the use of Programming by Demonstration (PbD) [7]. In [8] a model of the human motion is learned from demonstrations and encoded using a variant of DMP called Interaction Primitives (IP). Using IP the goal can be predicted. However, the adopted DMP representation does not preserve the spatial scaling properties of DMPs [9]. This can be a drawback when one wants to reproduce the same motion pattern scaled spatially to a different goal. In [10], Iterative Learning Control is employed to adjust the DMP's trajectory for transferring an object to a new position. However, this requires the repetition of the same transferring tasks until the true target position is reached. In [11] the idea of using an EKF is introduced to predict on-line the handover place and time of a DMP that parameterizes the human motion in handover tasks. However, in [11] the prediction is based on the current position of the human hand that is not physically coupled with the robot.

In this work we consider the problem of human-robot collaborative object transfer, where the robot is only aware of the pattern of motion, but is agnostic to the target position and how fast the movement should be executed (time scaling). The goal is to allow the human to execute the same motion pattern scaled to different targets and time scales, while anticipating the human's intention, making the robot proactive and minimizing the human's effort, by means of predicting the target position and time scaling. To tackle this problem we propose i) a model reference with a DMP based control input based on the desired (trained) pattern of motion and the estimates of the target position and time scaling, ii) an EKF-based observer for the estimation of the target position and time scaling with fading memory and parameter projection so that the estimation parameters respect certain bounds originating from their physical interpretation. As the human and robot are physically coupled, estimates are based on the interaction force and used in the control signal supplied to the robot. The physical coupling differentiates significantly the problem addressed in this work with respect to [11] since the overall system here consists of the robot controller and the observer under the exertion of the human

[1]Aristotle University of Thessaloniki, Department of Electrical and Computer Engineering, Thessaloniki 54124, Greece. antosidi@ece.auth.gr, doulgeri@eng.auth.gr

[2]Chalmers University of Technology, Department of Electrical Engineering, Göteborg, Sweeden. yiannis@chalmers.se

[a] This research is co-financed by Greece and the European Union (European Social Fund- ESF) through the Operational Programme Human Resources Development, Education and Lifelong Learning in the context of the project Strengthening Human Resources Research Potential via Doctorate Research (MIS-5000432), implemented by the State Scholarships Foundation (IKY)

[b] This research is co-financed by the Swedish Research Council (VR).

[c] The research leading to these results has received funding by the EU Horizon 2020 Research and Innovation Programme under grant agreement No 820767, project CoLLaboratE.

interaction force. Therefore the contribution of this work lies on the problem formulation, the design of the observer and robot controller and the proof of the stability of the overall system.

The remainder of this paper is structured as follows: Section II describes the proposed approach. A stability analysis is carried out in section III. In section IV experimental results are presented and discussed. Finally, section V provides a brief summary.

II. Proposed approach

We make use of DMP to encode the Cartesian position of the robot's end-effector during a point to point motion, that is recorded from a kinesthetic demonstration. This recorded motion pattern is employed by the robot for collaborative transportation of an object to different targets and at different time scalings unknown to the robot, which we will refer to as goal parameters. During the object transfer the robot and the human hold the object with a rigid grasp forming a rigid bond constraint. The object's weight is known and compensated by the robot. A model reference is proposed to drive a robot under velocity control. Using the current estimates of the goal parameters a DMP-based control signal is provided as input to the model reference. This control signal plays the role of the estimate of the desired acceleration, i.e. the acceleration that would be produced by the DMP with the ground-truth goal parameters and endows the robot with proactive behaviour. The force exerted by the human and measured by the F/T sensor is provided as a second input to the model reference, so that the human can intervene and enforce the desired acceleration. The discrepancy between the estimated and actual acceleration are used in an EKF-based observer to update the estimates of the goal parameters in order to ultimately converge to the actual ones, so that the human's intention can be inferred and no further or minimal intervention and effort is required by him.

In the following subsections we present the adopted DMP formulation, elaborate on the proposed scheme and detail the update of the goal parameters using an EKF-based observer.

A. Dynamic Movement Primitive

A DMP for encoding a point-to-point motion in Cartesian space is given by:

$$\tau^2 \ddot{\boldsymbol{y}} = \alpha_z \beta_z (\boldsymbol{g} - \boldsymbol{y}) - \alpha_z \tau \dot{\boldsymbol{y}} + g_f(x) \boldsymbol{f}(x) \tag{1}$$

$$\tau \dot{x} = 1 \ , \ x(0) = 0 \tag{2}$$

where $\boldsymbol{y}, \dot{\boldsymbol{y}}$ is the Cartesian position and velocity, $\boldsymbol{g}$ the target, x is the phase variable used to avoid direct dependency on time and $\tau > 0$ is a temporal scaling factor typically set equal to the demonstration's total duration. The forcing term $\boldsymbol{f}(x)$ is given by:

$$\boldsymbol{f}(x) = diag(\boldsymbol{g} - \boldsymbol{y}_0) \boldsymbol{f}_s(x) \tag{3}$$

where $\boldsymbol{y}_0$ is the initial position and $\boldsymbol{f}_s(x)$ is the weighted sum of N Gaussian kernels:

$$\boldsymbol{f}_s(x) = \frac{\sum_{i=1}^{N} \boldsymbol{W}_i \psi_i(x)}{\sum_{i=1}^{N} \psi_i(x)} \tag{4}$$

with $\psi_i(x) = exp(-h_i(x - c_i)^2)$, while $g_f(x)$ is a sigmoid gating function, ensuring the forcing term fades to zero at $x = 1$ as in [12]:

$$g_f(x) = \frac{1}{1 + e^{a_g(x - c_g)}} \tag{5}$$

In order for the linear part of (11) to be critically damped we choose $\alpha_z = \beta_z / 4 > 0$. The canonical system (2) can be any monotonically evolving function [13]. Here, we chose a linear canonical system to reduce the non-linearity of the DMP w.r.t τ, which affects the linearization done by the EKF in section II-C. The Gaussian kernels in (4) are spaced equally between 0 and 1 with centers $c_i = \frac{i-1}{N-1}$ and inverse widths $h_i = \frac{1}{(c_{i+1} - c_i)^2}$, $h_N = h_{N-1}$, $i = 1, \cdots, N$. The matrix $\boldsymbol{W} \in \mathbf{R}^{3 \times N}$, with $\boldsymbol{W}_i$ denoting the i_{th} column, contains in each row the weights for each Cartesian coordinate, which can be learned using Least Squares or Locally Weighted Regression (LWR) [14] based on the demonstrated data. Owning to (5) the forcing term eventually vanishes, thus (1) acts as a pure spring-damper and converges to the goal y_g. The parameters a_g, c_g are chosen so that $g(x) \approx 1$ for $x \in [0 \ , \ 1)$ (i.e. $t \in [0 \ , \ \tau)$) and $g(x)$ decreases quickly to 0 for $x \geq 1$ (i.e. $t \geq \tau$).

B. Control scheme

We consider a velocity controlled robot, therefore it is assumed that any reference velocity can be accurately tracked. Moreover, a F/T sensor is assumed to be mounted at its end-effector measuring external forces. The proposed scheme is presented in Fig. 1. The reference position $\boldsymbol{y}_r$ and velocity $\dot{\boldsymbol{y}}_r$ are outputs of a model reference, given by:

$$\boldsymbol{M}_r \ddot{\boldsymbol{y}}_r = \boldsymbol{u}_r + \boldsymbol{f}_{ext} \tag{6}$$

where $\boldsymbol{M}_r = diag(m_x, m_y, m_z) > 0$ is the reference model's inertia and is chosen such that it is not less than half the robot's actual inertia to ensure passivity [15]. The model reference accepts two inputs: (i) the external force $\boldsymbol{f}_{ext}$, which is assumed to be measured or calculated and (ii) a DMP based control input given by:

$$\boldsymbol{u}_r = \boldsymbol{M}_r \hat{\ddot{\boldsymbol{y}}} \tag{7}$$

where the signal $\hat{\ddot{\boldsymbol{y}}}$ is produced using the DMP equation (1) utilizing the current robot's reference position $\boldsymbol{y}_r$ and velocity $\dot{\boldsymbol{y}}_r$ and the estimates of the target $\hat{\boldsymbol{g}}$ and the time scaling $\hat{\tau}$:

$$\hat{\ddot{\boldsymbol{y}}} = \frac{1}{\hat{\tau}^2} \left(\alpha_z \beta_z (\hat{\boldsymbol{g}} - \boldsymbol{y}_r) - \alpha_z \hat{\tau} \dot{\boldsymbol{y}}_r + g(\hat{x}) \boldsymbol{f}(\hat{x}) \right) \tag{8}$$

where $\hat{x}$ is calculated by integrating (2) using the estimated time scaling $\hat{\tau}$. The generated signal in (8) is an estimated acceleration which would be equal to $\ddot{\boldsymbol{y}}_r$ if the actual target and time scaling were known and $\boldsymbol{f}_{ext}$ was zero.

The update of the estimation parameters $\hat{\boldsymbol{g}}$ and $\hat{\tau}$ is performed based on the external force $\boldsymbol{f}_{ext}$ using the EKF-based observer described in II-C.

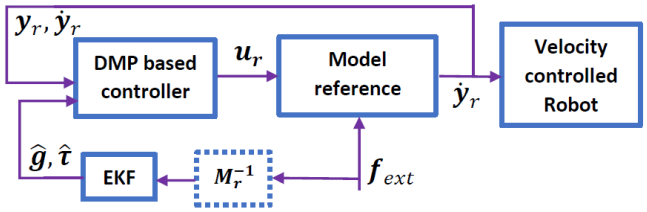

Fig. 1: Proposed approach.

C. EKF-based observer for target and time scale prediction

To estimate the target $\boldsymbol{g}$ and the time scaling τ we introduce the state vector $\boldsymbol{\theta} = \begin{bmatrix} \boldsymbol{g}^T & \tau \end{bmatrix}^T$. Assuming that the target and time scaling are constant we construct the following state equations:

$$\dot{\boldsymbol{\theta}} = \boldsymbol{0}_{4\times 1} \tag{9}$$

$$\ddot{\boldsymbol{y}} = \boldsymbol{h}_{\boldsymbol{\theta}}(\boldsymbol{\theta}, \boldsymbol{y}_r, \dot{\boldsymbol{y}}_r, t) \tag{10}$$

where $\ddot{\boldsymbol{y}}$ is the output and $\boldsymbol{h}_{\boldsymbol{\theta}}(\boldsymbol{\theta}, \boldsymbol{y}_r, \dot{\boldsymbol{y}}_r, t)$ is given by:

$$\begin{aligned} &\boldsymbol{h}_{\boldsymbol{\theta}}(\boldsymbol{\theta}, \boldsymbol{y}_r, \dot{\boldsymbol{y}}_r, t) = \\ &\frac{1}{\tau^2}\left(\alpha_z\beta_z(\boldsymbol{g} - \boldsymbol{y}_r) - \alpha_z\tau\dot{\boldsymbol{y}}_r + g(t/\tau)\boldsymbol{f}(t/\tau)\right) \end{aligned} \tag{11}$$

where we have substituted x with its analytic solution from (2). For the system given by (9)-(10) we construct the following observer based on the fading memory EKF [16], [17]:

$$\dot{\hat{\boldsymbol{\theta}}} = \boldsymbol{K}(\ddot{\boldsymbol{y}} - \hat{\ddot{\boldsymbol{y}}}) \tag{12}$$

$$\hat{\ddot{\boldsymbol{y}}} = \boldsymbol{h}_{\boldsymbol{\theta}}(\hat{\boldsymbol{\theta}}, \boldsymbol{y}_r, \dot{\boldsymbol{y}}_r, t) \tag{13}$$

where $\hat{\boldsymbol{\theta}}$ is the state estimate, $\boldsymbol{h}_{\boldsymbol{\theta}}(\hat{\boldsymbol{\theta}}, \boldsymbol{y}_r, \dot{\boldsymbol{y}}_r, t)$ is the right hand side of (8) and $\boldsymbol{K} \in \mathbb{R}^{4\times 3}$ is a time varying gain matrix given by:

$$\boldsymbol{K} = \boldsymbol{P}(t)\boldsymbol{C}^T(t)\boldsymbol{R}^{-1} \tag{14}$$

where $\boldsymbol{P}(t)$ is given by the solution of the the following Ricatti equation:

$$\dot{\boldsymbol{P}}(t) = 2a_p\boldsymbol{P}(t) - \boldsymbol{P}(t)\boldsymbol{C}^T(t)\boldsymbol{R}^{-1}\boldsymbol{C}(t)\boldsymbol{P}(t) + \boldsymbol{Q} \tag{15}$$

$a_p > 0$, $\boldsymbol{R}$, $\boldsymbol{Q}$ are the measurement and process noise covariance matrices and

$$\boldsymbol{C}(t) = \left.\frac{\partial \boldsymbol{h}_{\boldsymbol{\theta}}(\boldsymbol{\theta}, \boldsymbol{y}_r, \dot{\boldsymbol{y}}_r, t)}{\partial \boldsymbol{\theta}}\right|_{\boldsymbol{\theta}=\hat{\boldsymbol{\theta}}} \tag{16}$$

The analytic calculation of $\boldsymbol{C}(t)$ is similar to [11].

Notice that in our case (12) is not implementable since the parameters $\boldsymbol{\theta}$ in (10) are unknown and hence $\ddot{\boldsymbol{y}}$ is not directly available. However, we can interpret $\boldsymbol{f}_{ext}$ as the human's intention to enforce the desired acceleration $\ddot{\boldsymbol{y}}$ and consequently assume that $\ddot{\boldsymbol{y}} = \hat{\ddot{\boldsymbol{y}}} + \boldsymbol{M}_r^{-1}\boldsymbol{f}_{ext}$. Moreover, substituting (7) in (6) we get $\ddot{\boldsymbol{y}}_r = \hat{\ddot{\boldsymbol{y}}} + \boldsymbol{M}_r^{-1}\boldsymbol{f}_{ext}$, therefore we can substitute the difference $\ddot{\boldsymbol{y}} - \hat{\ddot{\boldsymbol{y}}}$ with $\ddot{\boldsymbol{y}}_r - \hat{\ddot{\boldsymbol{y}}} = \boldsymbol{M}_r^{-1}\boldsymbol{f}_{ext}$. Hence, (12) can be written as

$$\dot{\hat{\boldsymbol{\theta}}} = \boldsymbol{K}\boldsymbol{M}_r^{-1}\boldsymbol{f}_{ext} \tag{17}$$

which is implementable, as $\boldsymbol{f}_{ext}$ is measured.

The EKF's performance is heavily dependent on the error between the estimated and actual parameters, which considerably affects the accuracy of the linearization in (16). In many cases, if this error is large, the estimates will diverge or the convergence can be very slow. To avoid divergence we exploit the fact that the robot's workspace is constrained and the time scaling is also bounded. Thus the estimation parameters $\boldsymbol{\theta}$ should respect the constraints $\underline{\boldsymbol{\theta}} \leq \boldsymbol{\theta} \leq \bar{\boldsymbol{\theta}}$ or equivalently:

$$\boldsymbol{D}\boldsymbol{\theta} \leq \boldsymbol{d} \tag{18}$$

where $\boldsymbol{d} = [\bar{\boldsymbol{\theta}}^T \ \ -\underline{\boldsymbol{\theta}}^T]^T$ and $\boldsymbol{D} = \begin{bmatrix} \boldsymbol{I}_4 & -\boldsymbol{I}_4 \end{bmatrix}^T$. We use the active set method, i.e. the constraints that are active at the particular estimate $\hat{\boldsymbol{\theta}}$. Those active constraints satisfy $\bar{\boldsymbol{D}}\hat{\boldsymbol{\theta}} = \bar{\boldsymbol{d}}$ and $\bar{\boldsymbol{D}}_i\dot{\boldsymbol{\theta}}_1 > 0$, where $\bar{\boldsymbol{D}}_i$ is the i_{th} row of $\bar{\boldsymbol{D}}$ and $\bar{\boldsymbol{D}}, \bar{\boldsymbol{d}}$ are subset of the rows of $\boldsymbol{D}, \boldsymbol{d}$ respectively. Employing the projection based on the maximum probability approach [17], the constraint estimation can be obtained from $\dot{\hat{\boldsymbol{\theta}}} = \boldsymbol{N}\dot{\boldsymbol{\theta}}_1$ where $\boldsymbol{N} = \left(\boldsymbol{I}_4 - \boldsymbol{P}(t)\bar{\boldsymbol{D}}^T(\bar{\boldsymbol{D}}\boldsymbol{P}(t)\bar{\boldsymbol{D}}^T)^{-1}\bar{\boldsymbol{D}}\right)$ is the projection matrix and $\dot{\boldsymbol{\theta}}_1 = \boldsymbol{P}(t)\boldsymbol{C}(t)\boldsymbol{R}^{-1}\boldsymbol{M}_r^{-1}\boldsymbol{f}_{ext}$ is the unconstrained time derivative of the state estimate given by (17) and (14), In order to guarantee the boundedness of the observer's update law, irrespective of the boundedness of $\boldsymbol{y}_r, \dot{\boldsymbol{y}}_r$, we normalize $\boldsymbol{C}(t)$ with $\bar{\boldsymbol{C}}(t) = \boldsymbol{C}(t)/c_n$ where $c_n = \sqrt{1 + \lambda_{max}(\boldsymbol{C}(t)\boldsymbol{C}^T(t))}$ [18]. Hence, our parameters estimation update law is given by:

$$\dot{\hat{\boldsymbol{\theta}}} = \boldsymbol{N}\boldsymbol{P}(t)\bar{\boldsymbol{C}}(t)\boldsymbol{R}^{-1}\boldsymbol{M}_r^{-1}\frac{\boldsymbol{f}_{ext}}{c_n} \tag{19}$$

Finally, we impose the condition $\rho_1\boldsymbol{I} \leq \boldsymbol{P}(t) \leq \rho_2\boldsymbol{I}$, where $\rho_1, \rho_2 > 0$ and $\rho_1 < \rho_2$ are design constants. To respect the upper bound, we modify $\dot{\boldsymbol{P}}(t)$ from (15):

$$\dot{\boldsymbol{P}} = \begin{cases} 2a_p\boldsymbol{P}(t) + \boldsymbol{Q} \\ -\boldsymbol{P}(t)\bar{\boldsymbol{C}}^T(t)\boldsymbol{R}^{-1}\bar{\boldsymbol{C}}(t)\boldsymbol{P}(t) \quad , ||\boldsymbol{P}(t)|| \leq \rho_2 \\ \boldsymbol{0} \ , \ otherwise \end{cases} \tag{20}$$

and to ensure the lower bound is not violated we reset $\boldsymbol{P}(t)$ at the time instant t_r when $||\boldsymbol{P}(t)|| \leq \rho_1$:

$$\boldsymbol{P}(t_r^+) = \rho_0\boldsymbol{I} \tag{21}$$

where $\rho_0 > \rho_1$ is a design constant. So the final EKF-based observer with fading memory, parameters projection and covariance bounding is given by (19)-(21).

III. Stability Analysis

To study the boundedness and convergence of $\boldsymbol{y}_r$, $\dot{\boldsymbol{y}}_r$, $\hat{\boldsymbol{g}}$ and $\hat{\tau}$ we state and prove the following theorem:

Theorem 1: The model reference given by (6)-(8) along with the observer based on the EKF given by (19)-(21) ensures that $\boldsymbol{y}_r, \dot{\boldsymbol{y}}_r, \hat{\boldsymbol{g}}, \hat{\tau} \in \boldsymbol{L}_\infty$ if $\boldsymbol{f}_{ext} \in \boldsymbol{L}_\infty \cap \boldsymbol{L}_2$.

Proof: First of all, the proposed observer imposes the boundedness of the the observer's states through projection (18)-(19) [17], therefore $\hat{\boldsymbol{g}}, \hat{\tau} \in \boldsymbol{L}_\infty$. Using equations (6)-(8) we can write the model reference in the following form:

$$\hat{\tau}^2\ddot{\boldsymbol{y}}_r = -\alpha_z\beta_z\boldsymbol{y}_r - \alpha_z\hat{\tau}\dot{\boldsymbol{y}}_r + \hat{\tau}^2\boldsymbol{d} \tag{22}$$

where $\boldsymbol{d} = \frac{1}{\hat{\tau}^2}\left(\alpha_z\beta_z\hat{\boldsymbol{g}} + g(\hat{x})\boldsymbol{f}(\hat{x}) + \boldsymbol{M}_r^{-1}\boldsymbol{f}_{ext}\right)$ can be viewed as a time varying bounded disturbance since $\hat{\tau}, \hat{\boldsymbol{g}}, \boldsymbol{f}_{ext} \in \boldsymbol{L}_\infty$ and $\boldsymbol{f}(\hat{x}) \in \boldsymbol{L}_\infty$ for $\hat{\boldsymbol{g}}, \hat{\tau} \in \boldsymbol{L}_\infty$. The system in (22) can be decoupled in each dimension, so will carry out the analysis in one dimension which we will denote by y and the same results hold for the rest. Therefore, we have:

$$\hat{\tau}^2\ddot{y} = -\alpha_z\beta_z y - \alpha_z\hat{\tau}\dot{y} + \hat{\tau}^2 d \tag{23}$$

Introducing the state variable $\boldsymbol{\zeta} = [y\ \dot{y}]^T$ (23) can be written in matrix form:

$$\dot{\boldsymbol{\zeta}} = \boldsymbol{A}(t)\boldsymbol{\zeta} + \boldsymbol{B}d \tag{24}$$

where $\boldsymbol{A}(t) = \frac{1}{\hat{\tau}^2}\begin{bmatrix} 0 & 1 \\ -\alpha_z\beta_z & -\alpha_z\hat{\tau} \end{bmatrix}$ and $\boldsymbol{B} = \begin{bmatrix} 0 \\ 1 \end{bmatrix}$. Since $\alpha_z, \beta_z > 0$ and $\hat{\tau}$ is positive and bounded, $Re\{\lambda_i(\boldsymbol{A}(t))\} \leq \sigma_s\ \forall t \geq 0,\ i = 1...4$, where $\sigma_s > 0$ is constant. Taking into account that $\bar{\boldsymbol{C}}(t), \boldsymbol{P}(t) \in \boldsymbol{L}_\infty$ and $\boldsymbol{f}_{ext} \in \boldsymbol{L}_\infty \cap \boldsymbol{L}_2$ it follows from (19) that $\dot{\hat{\tau}} \in \boldsymbol{L}_\infty \cap \boldsymbol{L}_2$. Therefore we also have $||\dot{\boldsymbol{A}}(t)|| \in \boldsymbol{L}_2$, since $||\boldsymbol{A}(t)|| = f_1(\hat{\tau}) > 0$, $||\dot{\boldsymbol{A}}(t)|| = \frac{\partial f_1(\hat{\tau})}{\partial \hat{\tau}}\dot{\hat{\tau}} \in \boldsymbol{L}_2$ because $\frac{\partial f_1(\hat{\tau})}{\partial \hat{\tau}} \in \boldsymbol{L}_\infty$ and $\dot{\hat{\tau}} \in \boldsymbol{L}_2$. Finally, since $\boldsymbol{A}(t)$ is differentiable and bounded and we can utilize Theorem 3.4.11 from [18] to show that the origin is uniformly globally asymptotically stable equilibrium for the system $\dot{\boldsymbol{\zeta}} = \boldsymbol{A}(t)\boldsymbol{\zeta}$. Therefore there exist matrices $\boldsymbol{\Pi}(t) = \boldsymbol{\Pi}^T(t) > 0$ and $\boldsymbol{Q}(t) = \boldsymbol{Q}^T(t) > 0$ with $\dot{\boldsymbol{\Pi}} = -\boldsymbol{A}^T(t)\boldsymbol{\Pi}(t) - \boldsymbol{\Pi}(t)\boldsymbol{A}(t) - \boldsymbol{Q}(t)$ satisfying $0 < \pi_1 < ||\boldsymbol{\Pi}(t)|| < \pi_2$ and $0 < q_1 < ||\boldsymbol{Q}(t)|| < q_2$. Therefore the system (24) is uniformly ultimately bounded, which can be shown easily using the Lyapunov function $V = \boldsymbol{\zeta}^T\boldsymbol{\Pi}(t)\boldsymbol{\zeta}$. Hence, $y, \dot{y} \in \boldsymbol{L}_\infty$. The same analysis holds for each dimension of $\boldsymbol{y}_r$, so $\boldsymbol{y}_r, \dot{\boldsymbol{y}}_r \in \boldsymbol{L}_\infty$, which concludes the proof of the theorem. ■

Moreover, the local exponential convergence of the target and time scaling predictions using EKF based on DMPs has been studied in [11]. If the necessary conditions for local exponential convergence are satisfied it can further be shown that $\hat{\boldsymbol{g}} \to \boldsymbol{g}$ and $\hat{\tau} \to \tau$ [11]. Then we also have that $\boldsymbol{f}_{ext} \to 0$ (otherwise $\dot{\boldsymbol{\theta}} \neq \boldsymbol{0}$ which contradicts the assumption $\hat{\boldsymbol{g}} \to \boldsymbol{g}$ and $\hat{\tau} \to \tau$) hence $\boldsymbol{d} \to \frac{1}{\tau}^2\alpha_z\beta_z\boldsymbol{g}$, so it can be easily shown that for the system (24) we will have $\boldsymbol{y}_r \to \boldsymbol{g}$ and $\dot{\boldsymbol{y}}_r \to \boldsymbol{0}$.

IV. Experimental results

The experimental setup consisted of a Kuka LWR4+ robot equipped with an ATI F/T sensor and a Barrett Hand. The training phase consisted of a single demonstration to a fixed target $\boldsymbol{g}_0$, from the initial position $\boldsymbol{y}_0$, by kinesthetically guiding the robot and recording its Cartesian position. These data were used to train a DMP. Testing was then performed to three different targets, $\boldsymbol{g}_1, \boldsymbol{g}_2, \boldsymbol{g}_3$ unseen to the robot. The robot was under velocity control driven by the Cartesian reference velocity $\dot{\boldsymbol{y}}_r$, keeping its orientation constant. The control cycle was $2ms$. The robot and the user were holding a small box whose weight was known. The user was instructed to transfer the box to a new fixed target, unknown to the robot, as shown in Fig. 2. The force was measured by the F/T sensor and the weight of the box was subtracted from the measurement along the gravity direction to retrieve the human exerted force, $\boldsymbol{f}_{ext}$. Throughout the experiments the initial position was $\boldsymbol{y}_0 = [0.02,\ 0.39,\ 0.16]^T$, the initial target estimate $\hat{\boldsymbol{g}}(0) = \boldsymbol{g}_0 = [0.18,\ 0.65,\ 0.35]^T$ and the new targets for each of the three experiments was $\boldsymbol{g}_1 = [-0.24,\ 0.68,\ 0.59]^T$, $\boldsymbol{g}_2 = [-0.33,\ 0.63,\ 0.19]^T$ and $\boldsymbol{g}_3 = [-0.03,\ 0.64,\ 0.62]^T$ respectively. The parameters chosen for the DMP were $N = 20$, $\alpha_z = 20$, $\beta_z = 5$, for the model reference $\boldsymbol{M}_r = 5\boldsymbol{I}_3$ and for the observer $P_0 = \boldsymbol{I}_4$, $R = 1\boldsymbol{I}_3$, $Q = 0.005\boldsymbol{I}_4$, $a_p = 1.002$, $\rho_0 = 1.0$, $\rho_1 = 0.01$, $\rho_2 = 1000$, $\bar{\boldsymbol{\theta}} = [0.65\ 0.8\ 0.7\ 60]^T$, $\underline{\boldsymbol{\theta}} = [-0.65\ 0.05\ 0.15\ 1.5]^T$. For the EKF the discrete implementation was employed [17].

The proposed approach was also compared to using only a pure admittance, i.e. $\boldsymbol{M}\ddot{\boldsymbol{y}} + \boldsymbol{D}\dot{\boldsymbol{y}} = \boldsymbol{f}_{ext}$, where $\boldsymbol{M} = 5\boldsymbol{I}_3$ and $\boldsymbol{D} = 10\boldsymbol{I}_3$, were tuned manually for best performance. The comparison was based on three metrics: 1) the total absolute work $\int_0^T ||\boldsymbol{f}_{ext}^T\dot{\boldsymbol{y}}||dt$, where T is the total movement duration, 2) the total power of the signal $\boldsymbol{f}_{ext}$, i.e. $\int_0^T ||\boldsymbol{f}_{ext}||^2 dt$ and 3) the Euclidean norm of the error between the target estimate and the ground-truth target (since for the admittance we don't have a target estimate we use the robot's final position instead).

Two users were involved, where the first one had prior experience with robots, while the second did not. Both users were given some time to get accustomed to the setup and feel more comfortable with it. The users were instructed to avoid direct contact at the target to forego generating additional external forces owing to contact.

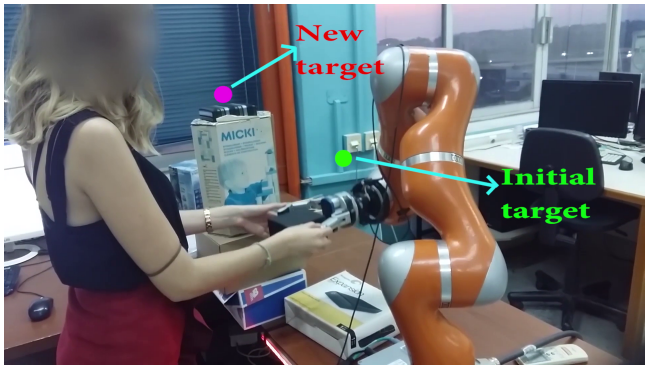

Fig. 2: Experimental setup.

TABLE I: Work, power of $\boldsymbol{f}_{ext}$ and Euclidean norm of the error between the ground-truth and estimated target for the proposed scheme and the admittance in each of the three experiments for both users.

Exp#	Method	$\int_0^T ||\boldsymbol{f}_{ext}^T\dot{\boldsymbol{y}}||dt$		$\int_0^T ||\boldsymbol{f}_{ext}||^2 dt$		$||\boldsymbol{g} - \hat{\boldsymbol{g}}||$ (cm)	
		usr1	usr2	usr1	usr2	usr1	usr2
1	DMP+EKF	0.21	0.24	2.63	3.77	0.4	0.4
	admittance	1.49	1.29	20.33	17.2	1.1	1.8
2	DMP+EKF	0.13	0.09	4.17	1.9	1.2	1.5
	admittance	0.82	0.81	11.5	11.7	1.1	1.9
3	DMP+EKF	0.27	0.22	3.53	2.9	1.1	0.9
	admittance	1.32	1.23	18.47	16.57	1.8	1.4

The aggregate results for both users are presented in Table I where the label DMP+EKF denotes the proposed approach.

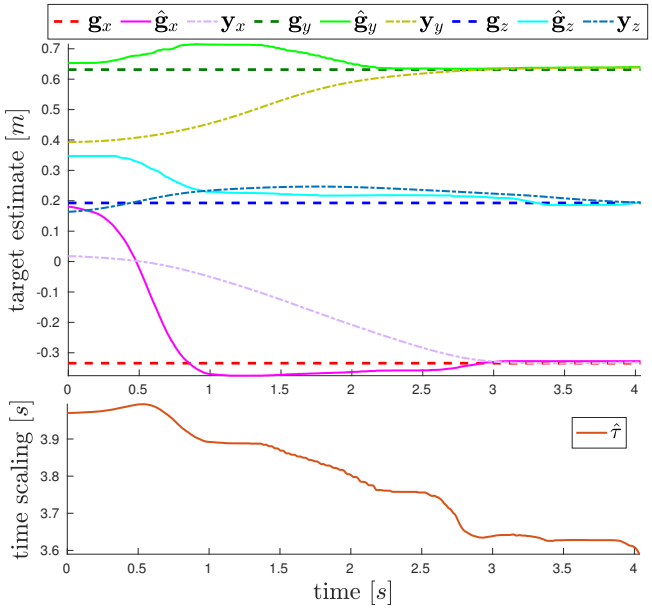

Fig. 3: Estimation results from experiment 2 for user 1. The top plot presents the target position estimation. The solid lines with colors red, green and blue for the x, y and z coordinates respectively are the estimates and the dashed lines the actual ones. The robot's position is plotted as well with dash-dotted line. The bottom plot presents the time scaling estimate.

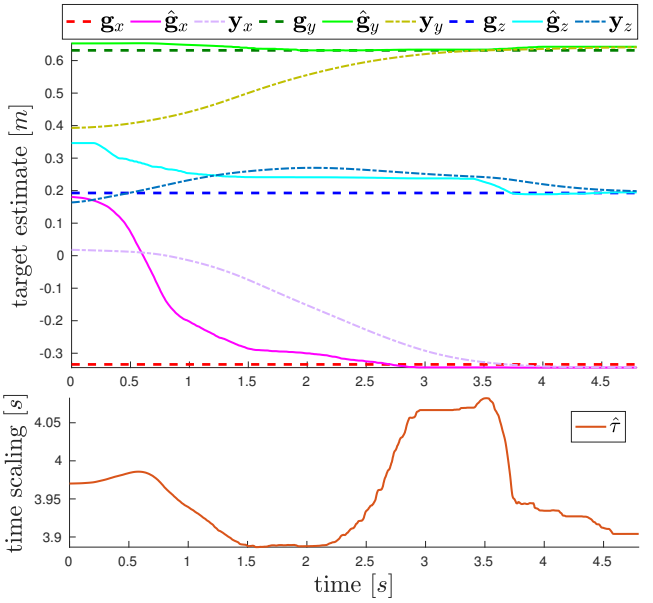

Fig. 5: Estimation results from experiment 2 for user 2. The top plot presents the target position estimation. The solid lines with colors red, green and blue for the x, y and z coordinates respectively are the estimates and the dashed lines the actual ones. The robot's position is plotted as well with dash-dotted line. The bottom plot presents the time scaling estimate.

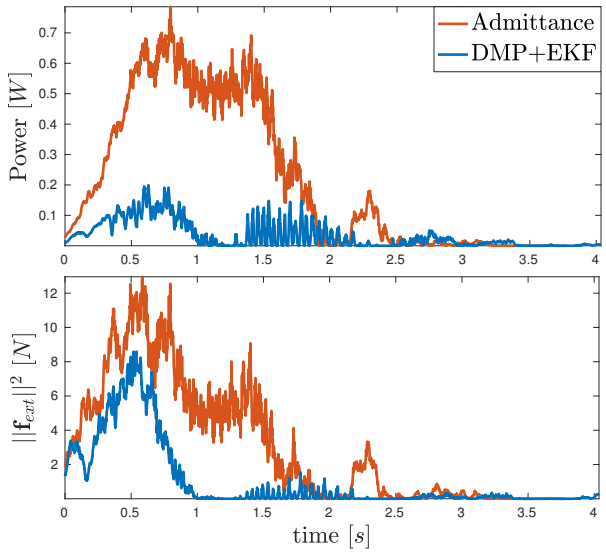

Fig. 4: Effort by user 1 in experiment 2. In the first row the power is plotted with blue line for using the DMP+EKF prediction and is compared with using only admittance (light brown line). In the second row the squared norm of the human's force is plotted again for both cases.

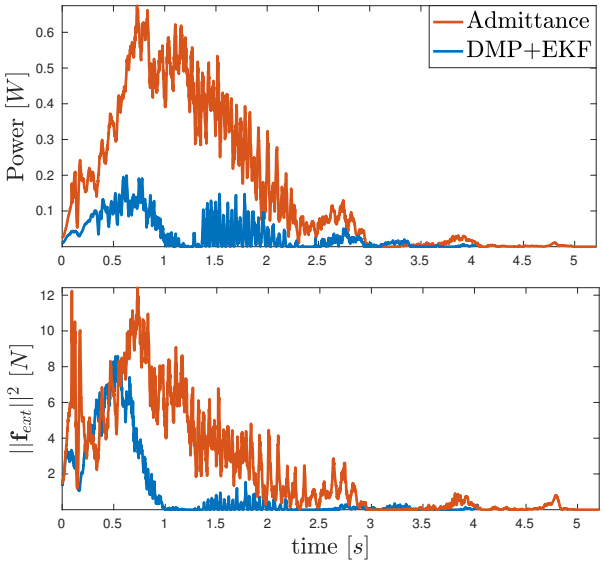

Fig. 6: Effort by user 2 in experiment 2. In the first row the power is plotted with blue line for using the DMP+EKF prediction and is compared with using only admittance (light brown line). In the second row the squared norm of the human's force is plotted again for both cases.

From this table we can see that the results of both users for the same experiment and method are quite similar, therefore the inexperienced user (user 2) performed equally well with the experienced one (user 1). Moreover, it is clear that the proposed method significantly outperforms the admittance in terms of effort (work and power), while the final target error is comparable in both cases and within the allowable

tolerance. Indicatively, the target and time scaling estimates are given in Fig. 3,5 with quantities related to x, y and z coordinate are plotted with red, green and blue respectively. The ground-truth targets are plotted with dashed lines, the target estimates with solid lines and the robot's position with dashed-dotted lines. The time scaling estimate is plotted with solid light brown line (notice that there is no ground-truth value). In Fig. 4, 6 the corresponding effort by the human is presented by plotting the instantaneous power and the squared norm of the interaction force, both for the proposed scheme and for using only admittance. In Fig. 3,5 we can see that the estimated target position converges quite fast to a small region close to the groundtruth target for both users. This can be discerned more clearly in the x axis where we have the larger error between the inital estimate and the groundtruth target. Moreover, for user 1 there is a small overshoot in x and y coordinates of the target estimates. This is in line with the higher forces he exerted in Fig. 4 during the time span where the overshoot occurs compared to the corresponding forces in Fig. 6 of the second user, for whom no overshoot occurs as can be seen in Fig 5. Finally, the effort pattern in Fig. 3,5 for the proposed method is compatible with that of the admittance (i.e. higher forces at the beginning and during the tranfer fading to zero at the end) however with smaller magnitude as less effort is required by the human.

A video with the experiments can be found in https://youtu.be/OU0W1-wBbg8.

V. Conclusions

In this work a model reference with a DMP-based control input and an EKF-based observer for predicting the target and time scaling was proposed in collaborative human-robot object transfer. The proposed scheme is shown theoretically to be globally stable and locally exponentially convergent to the final target estimate under bounded external forces with finite energy. Experimental results validate the proposed approach and exhibit its practical merits in terms of human effort reduction. In this work the object's weight was assumed known beforehand and only human exerted forces were considered. However, in a complete object transfer scenario, the object's weight may not be known a priori and contact with the environment when placing the object will inevitably occur, resulting in additional forces. Our future work will extend the proposed method to include orientation and incorporate unknown object dynamics.

References

[1] B. Chandrasekaran and J. M. Conrad, "Human-robot collaboration: A survey," in *SoutheastCon 2015*, April 2015, pp. 1–8.

[2] S. Miossec and A. Kheddar, "Human motion in cooperative tasks: Moving object case study," in *2008 IEEE International Conference on Robotics and Biomimetics*, Feb 2009, pp. 1509–1514.

[3] N. Jarrasse, J. Paik, V. Pasqui, and G. Morel, "How can human motion prediction increase transparency?" in *2008 IEEE International Conference on Robotics and Automation*, May 2008, pp. 2134–2139.

[4] Y. Maeda, T. Hara, and T. Arai, "Human-robot cooperative manipulation with motion estimation," in *Proceedings 2001 IEEE/RSJ International Conference on Intelligent Robots and Systems. Expanding the Societal Role of Robotics in the the Next Millennium (Cat. No.01CH37180)*, vol. 4, 2001, pp. 2240–2245 vol.4.

[5] B. Corteville, E. Aertbelien, H. Bruyninckx, J. D. Schutter, and H. V. Brussel, "Human-inspired robot assistant for fast point-to-point movements," in *Proceedings 2007 IEEE International Conference on Robotics and Automation*, April 2007, pp. 3639–3644.

[6] T. Flash and N. Hogans, "The coordination of arm movements: An experimentally confirmed mathematical model," *Journal of neuroscience*, vol. 5, pp. 1688–1703, 1985.

[7] A. Billard, S. Calinon, R. Dillmann, and S. Schaal, *Robot Programming by Demonstration*. Berlin, Heidelberg: Springer Berlin Heidelberg, 2008, pp. 1371–1394.

[8] G. Maeda, M. Ewerton, R. Lioutikov, H. B. Amor, J. Peters, and G. Neumann, "Learning interaction for collaborative tasks with probabilistic movement primitives," in *2014 IEEE-RAS International Conference on Humanoid Robots*, Nov 2014, pp. 527–534.

[9] A. J. Ijspeert, J. Nakanishi, H. Hoffmann, P. Pastor, and S. Schaal, "Dynamical movement primitives: Learning attractor models for motor behaviors," *Neural Comput.*, vol. 25, no. 2, pp. 328–373, Feb 2013.

[10] A. Gams, B. Nemec, A. J. Ijspeert, and A. Ude, "Coupling movement primitives: Interaction with the environment and bimanual tasks," *IEEE Transactions on Robotics*, vol. 30, no. 4, pp. 816–830, Aug 2014.

[11] D. Widmann and Y. Karayiannidis, "Human motion prediction in human-robot handovers based on dynamic movement primitives," in *European Control Conference*, June 2018.

[12] T. Kulvicius, K. Ning, M. Tamosiunaite, and F. Worgtter, "Joining movement sequences: Modified dynamic movement primitives for robotics applications exemplified on handwriting," *IEEE Transactions on Robotics*, vol. 28, no. 1, pp. 145–157, Feb 2012.

[13] A. Paraschos, C. Daniel, J. R. Peters, and G. Neumann, "Probabilistic movement primitives," in *Advances in Neural Information Processing Systems 26*, C. J. C. Burges, L. Bottou, M. Welling, Z. Ghahramani, and K. Q. Weinberger, Eds. Curran Associates, Inc., 2013, pp. 2616–2624.

[14] S. Schaal and C. G. Atkeson, "Constructive incremental learning from only local information," *Neural Comput.*, vol. 10, no. 8, pp. 2047–2084, Nov. 1998.

[15] B. Lacevic and P. Rocco, "Closed-form solution to controller design for human-robot interaction," *Journal of Dynamic Systems, Measurement, and Control*, vol. 133, no. 2, p. 024501, 2011.

[16] K. Reif, F. Sonnemann, and R. Unbehauen, "An ekf-based nonlinear observer with a prescribed degree of stability," *Automatica*, vol. 34, no. 9, pp. 1119 – 1123, 1998.

[17] D. Simon, *Optimal State Estimation: Kalman, H Infinity, and Nonlinear Approaches*. New York, NY, USA: Wiley-Interscience, 2006.

[18] P. A. Ioannou and J. Sun, *Robust Adaptive Control*. Upper Saddle River, NJ, USA: Prentice-Hall, Inc., 1995.